ACS NANO

www.acsnano.org

ARTICLE

A Wireless, Regeneratable Cocaine Sensing Scheme Enabled by Allosteric Regulation of pH Sensitive Aptamers

Shulin Chen, Tzu-Li Liu, Yan Dong, and Jinghua Li*

Cite This: *ACS Nano* 2022, 16, 20922–20936

Read Online

ACCESS | Metrics & More | Article Recommendations | Supporting Information

ABSTRACT: A key challenge for achieving continuous biosensing with existing technologies is the poor reusability of the biorecognition interface due to the difficulty in the dissociation of analytes from the bioreceptors upon surface saturation. In this work, we introduce a regeneratable biosensing scheme enabled by allosteric regulation of a re-engineered pH sensitive anti-cocaine aptamer. The aptamer can regain its affinity with target analytes due to proton-promoted duplex-to-triplex transition in DNA configuration followed by the release of adsorbed analytes. A Pd/PdH$_x$ electrode placed next to the sensor can enable the pH regulation of the local chemical environment via electrochemical reactions. Demonstration of a "flower-shaped", stretchable, and inductively coupled electronic system with sensing and energy harvesting capabilities provides a promising route to designing wireless devices in biointegrated forms. These advances have the potential for future development of electronic sensing platforms with on-chip regeneration capability for continuous, quantitative, and real-time monitoring of chemical and biological markers.

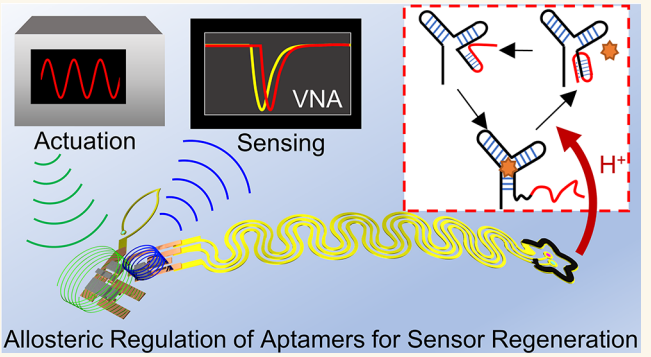

KEYWORDS: *allosteric DNA, aptamers, regeneratable biosensors, flexible electronics, inductive coupling*

Downloaded via OHIO STATE UNIV on May 8, 2023 at 12:35:30 (UTC).
See https://pubs.acs.org/sharingguidelines for options on how to legitimately share published articles.

One common goal shared by research in biosensing, analytical chemistry, and biointegrated electronics is to develop designs and integration schemes for sensors that support quantitative and real-time monitoring of biomarker concentrations in multiple bodily fluids such as saliva, blood, interstitial fluids, urine, and others.[1−4] Conventional biosensing techniques, such as enzyme-linked immunosorbent assay (ELISA), capillary electrophoresis (CE), gas chromatography (GC), and high-performance liquid chromatography (HPLC),[5−7] require the use of centralized equipment and trained personnel for operation, and thus are not compatible with continuous monitoring in home, community, and workplace settings. To this end, label-free biosensors with functionalized biochemical interfaces provide a realistic route for the rapid detection of biomarkers in complex environments.[8] Nevertheless, the bottleneck for continuous monitoring using biosensor chips is in the reusability of the immobilized biorecognition elements. Pioneering studies report the regeneration of biochemical sensors through regrafting biorecognition elements after usage. These methods, however, rely on additional chemical reagents for surface cleaning followed by refunctionalization of the devices and, therefore, are not compatible with building in vivo biosensors for continuous monitoring.[9,10] Removal of adsorbed biomarkers through electrochemical reactions/electrical repulsion serves a promising strategy for in situ regeneration but may require delicate design of the sensing interfaces consisting of multiple functional layers such as molecularly imprinted polymers and redox-active nanoreporters.[11] In vitro selected aptamers enabled by the systematic evolution of ligands by exponential enrichment (SELEX),[4,12−15] on the other hand, provide attractive opportunities for developing reusable sensors due to the reconfigurable nature of DNA sequences. However, while their noncovalent interactions with the corresponding targets (e.g., hydrogen bonds, electrostatic bonds, van der Waals forces) are reversible in nature, most methods that previous works report for dissociating targets from aptamers exploit extreme conditions, such as with

Received: August 25, 2022
Accepted: November 29, 2022
Published: December 5, 2022

ACS Publications

© 2022 American Chemical Society

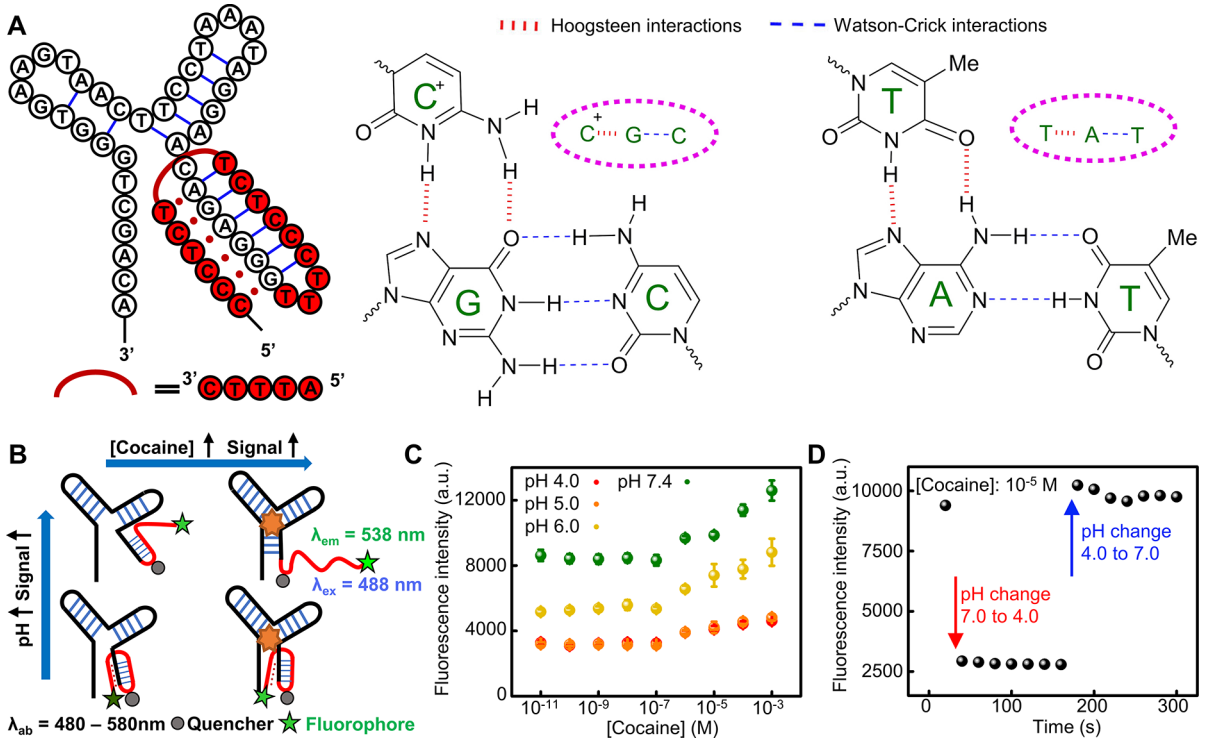

Figure 1. Regeneration mechanism of the pH sensitive anti-cocaine aptamer based on allosteric regulation. (A) DNA sequence of the re-engineered anti-cocaine aptamer used in this study. The aptamer has a pH sensitive motif at the 5′ end enabling the reversible duplex-to-triplex switch through the formation of intramolecular Hoogsteen interactions in acidic environment. (B) Schematic illustration of the conformational change of the pH sensitive aptamer labeled with a fluorophore and a quencher. The fluorescence intensity resulting from the interaction between the fluorophore and quencher serves as a measure for characterizing the conformation. (C) Fluorescence intensity of the labeled anti-cocaine aptamer responding to test solutions with varying pH values (4.0 to 7.4) and cocaine concentrations (10^{-11} to 10^{-3} M). (D) Real-time fluorescence intensity of the aptamer to dynamic changes in pH values (cocaine concentration: 10^{-5} M) showing the fast response time.

heating,[16] ultraviolet light exposure,[17,18] and concentrated chemicals.[19] Consequently, most biosensors still have a limited capability for repetitive use due to the surface saturation issue. The knowledge gap highlights the crucial need for establishing general sensing schemes that allow for the regeneration of biosensor surfaces and continuous monitoring of biomolecules.

To this end, the allosteric regulation of triplex nucleic acid helices has offered opportunities in controlling the affinity between ligands and receptors and thus has received considerable attention as a rich "toolbox" for multiple purposes. Briefly, this strategy utilizes DNA sequence(s) capable of assembling into an inter- or intramolecular triplex structure through Hoogsteen interactions in acidic environments.[20] Interest in fundamental aspects of the design of aptamers and their applications in different areas (e.g., nanomachines, logic circuits, stimuli-responsive hydrogels)[21−23] has motivated continued research efforts in this field. In particular, pioneering studies suggest that the pH-induced, switchable duplex-to-triplex transition can result in the disruption of the stem-loop structure of aptamers within a short time (<100 s) followed by the release of binding ligands.[24,25] Despite the great success in this field, the design principles and integration schemes based on this concept for creating biointegrated electronics are worth further study.

This study reports an engineering solution to the challenge in continuous biosensing by using allosteric DNA-based aptamers as the sensing interface for electronic biosensors. As an example, cocaine is a highly addictive stimulant drug, and the abuse of it may cause instantaneous adverse effects on the human body, including tachycardia, hypertension, anxiety, organ damage, and immunodeficiency.[26,27] Motivated by the need for sensing platforms monitoring the concentration of cocaine, this study exploits a re-engineered anti-cocaine aptamer with a pH sensitive domain introduced to the original ligand recognition sequence[28−30] to establish the proof-of-concept of regeneratable biosensors.[24] Results suggest that an allosteric DNA-functionalized surface shows pH tunable performance and can restore the sensing capability via the proper treatment of the interface in a proton-rich environment. Inspired by recent successes on electrical signal-mediated release of drugs/chemicals[31,32] to form communication loops, placing a pH regulating Pd electrode close to the sensing interface can reversibly and focally control the pH value of the microenvironment, triggering the regeneration while ensuring a minimal perturbation to surrounding areas. Inductively coupling the biochemical interface to a custom-designed signal transducer and energy harvesting system allows for wireless sensing/pH regulation. Together, the design principles, materials selections, circuit layout, and integration scheme provide a realistic and promising route to building regenerat-able biochemical sensors, which can potentially be adapted to different aptamer-mediated sensing systems. The major contribution of this work is the development of a method that enables in situ sensor regeneration under mild and biocompatible conditions together with the supporting wireless sensing/actuation schemes. The system can find potential applications for in vivo, continuous biosensing.

https://doi.org/10.1021/acsnano.2c08511
ACS Nano 2022, 16, 20922−20936

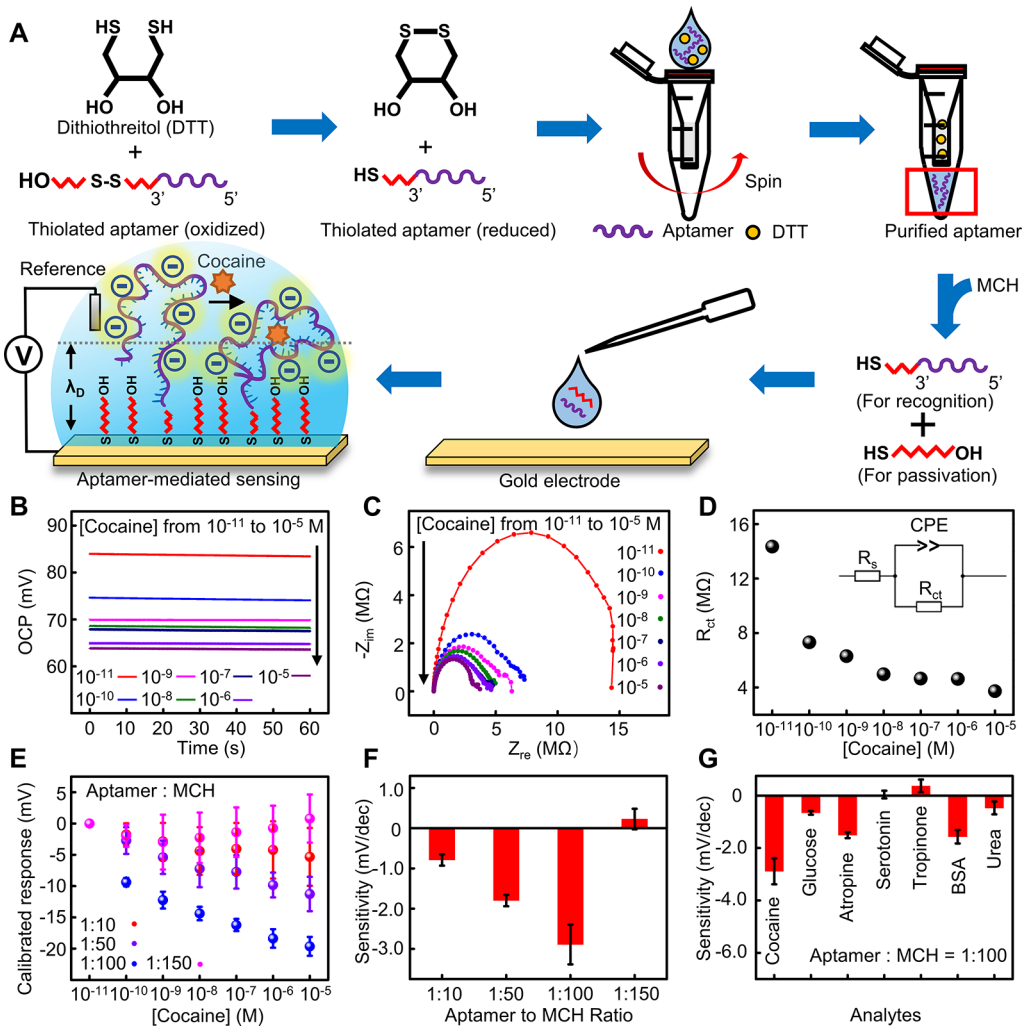

Figure 2. Design, preparation, and characterization of potentiometric anti-cocaine sensing platforms based on the pH sensitive aptamer. (A) Fabrication procedures for the aptamer-functionalized sensor for cocaine detection. (B) Open circuit potential of the resulting potentiometric sensors in 1× PBS solutions with different concentrations of cocaine ranging from 10^{-11} to 10^{-5} M (after signal stabilization). (C) EIS characterization (Nyquist plot) of a sensing electrode in 1× PBS solutions with different concentrations of cocaine. (D) Extracted charge transfer resistance based on results in C. (E) Calibrated response plots of sensing electrodes with different ratios of aptamer to MCH used for surface functionalization. (F) Extracted sensitivities of electrodes with different aptamer-to-MCH ratios based on results in E. (G) Comparison of responses of the anti-cocaine sensors to cocaine and potential interferents including glucose, atropine, serotonin, tropinone, BSA, and urea.

RESULTS AND DISCUSSION

Characterization of pH Sensitive, Allosteric Anti-Cocaine Aptamer. The study uses a re-engineered DNA containing a pH sensitive domain at the 5′ end distal from the classic cocaine recognition sequence (Figure 1A, left).[29,33] The motif consists of two self-complementary sequences separated by a loop and is capable of self-assembling with the stem of the recognition sequence into an intramolecular triplex structure through parallel Watson−Crick and Hoogsteen interactions between base pairs (i.e., CGC^+/TAT). For a CG-rich sequence, the formation of a stable triplex is energetically more favorable in acidic environments due to the need for protonated cytosine (at the N3 site) for the Hoogsteen interaction. With a decreasing pH, the self-assembly of the intramolecular triplex disrupts the stem of the cocaine−aptamer complex with a three-way junction structure, leading to the release of ligands. At higher pH values, on the other hand, the unfolding of the triplex due to the lack of hydrogen bonds restores the function of the aptamer for cocaine binding.

Labeling the DNA strand with fluorescence resonance energy transfer (FRET) pairs allows for the characterization of the dynamic conformational change of the aptamer in response to varying cocaine concentrations and pH values (Figure 1B). Placing the fluorophore (ATTO488) and Black Hole Quencher-1 (BHQ-1) at different locations in the sequence can enable the visualization of the reversible duplex-to-triplex transition by measuring the fluorescence emission spectrum in the wavelength range from 530 to 550 nm with an excitation wavelength of ∼488 nm. Consistent with the mechanism described in Figure 1B, a lower pH promotes the formation of the triplex, resulting in a decreased fluorescence intensity by bringing the fluorophore closer to the quencher, and vice versa (Figure 1C). The cocaine concentration also affects the conformation by competing with the pH sensitive motif for interacting with the stem part in the cocaine recognition sequence. As a result, increasing the concentration of cocaine suppresses the transition to the triplex, leading to an enhanced fluorescence intensity with the same pH value in

https://doi.org/10.1021/acsnano.2c08511
ACS Nano 2022, 16, 20922−20936

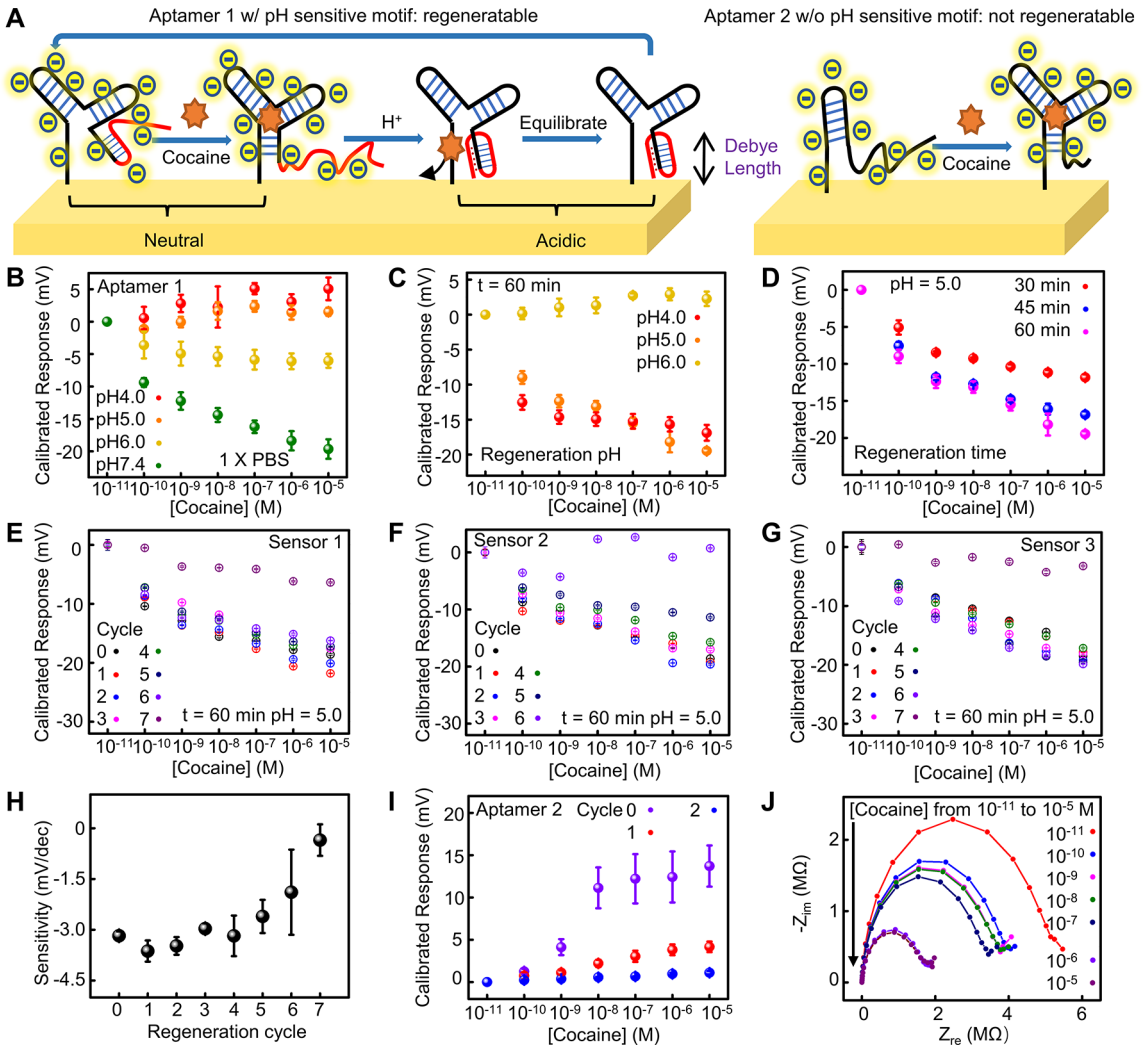

Figure 3. Characterization of the regeneration behavior of the pH sensitive aptamer sequence through allosteric regulation. (A) Working principle of the pH-induced sensing surface regeneration. At neutral pH, the anti-cocaine aptamer with pH sensitive motif (Aptamer 1) has an affinity to its target and can fold into a three-way junction upon binding. As pH decreases, the triplex formation at the 5′ end disrupts the stem structure, inhibits binding, and facilitates the release of cocaine molecules. In contrast, the DNA sequence without the pH sensitive motif (Aptamer 2) lacks the capability of regeneration. (B) Calibrated response of the anti-cocaine sensors with Aptamer 1 (in mV) as a function of cocaine concentration in 1× PBS with different pH values. The curve at pH = 7.4 uses the same data in Figure 2E (aptamer to MCH ratio = 1:100) for comparison. (C) Calibrated response plots of saturated anti-cocaine sensors regenerated in solution with pH values of 4.0, 5.0, and 6.0 for 60 min, respectively. (D) Calibrated response plots of saturated anti-cocaine sensors regenerated in 1× PBS solution (pH = 5.0) for 30, 45, and 60 min, respectively. The curve for 60 min uses the same data in C (pH = 5.0, 60 min) for comparison. (E, F, G) Sequential display of sensing performance of three anti-cocaine sensors before and after repetitive regeneration cycles (pH = 5.0, 60 min). (H) Summary of average sensitivity extracted from E−G as a function of the number of regeneration cycle (0−7). (I) Sensing performance of anti-cocaine sensors functionalized with Aptamer 2 during repetitive regeneration cycles. (J) EIS characterization (Nyquist plot) of a sensing electrode with Aptamer 2 in 1× PBS solutions with different concentrations of cocaine.

cases examined here (pH from 4.0 to 7.4). The transition between duplex and triplex is transient and reversible (Figure 1D): adjusting the pH values (between 4.0 and 7.0) induces an instant change in the fluorescence signal, which goes back upon the reverse of the pH to the original value. To further demonstrate the reversible, dynamic duplex-to-triplex transition process in cocaine solution with a concentration of 10^{-5} M, Video S1 shows the real-time fluorescence emission intensity (excitation and emission wavelength range: 450−490 and 500−540 nm, 5× speed) captured by a microscope (EVOS M5000, ThermoFisher). Results suggest that the fluorescence intensity decreases immediately following a lowering in the pH value (pH 5.0) of the environment and increases when the pH goes back to neutral (pH 7.0). Repeating this process for multiple cycles confirms the reversibility of the conformational alternation. The results are consistent with previous studies,[29] and thus, serve as the foundation for the design of regeneratable electronic biosensors in the following sections.

Design of Anti-Cocaine Aptamer Functionalized Sensing Interfaces. Modifying electrode surfaces with aptamers as the biorecognition elements enables the generation of a quantifiable electric voltage signal that scales with the concentration of target analytes. A schematic illustration of the preparation and working principle of an aptamer-functionalized cocaine sensor appears in Figure 2A. The interaction between target molecules and the corresponding aptamers can induce a conformational rearrangement of

https://doi.org/10.1021/acsnano.2c08511
ACS Nano 2022, 16, 20922−20936

the single-stranded DNA with negatively charged phosphodiester backbones.[4] Consequently, the perturbation in surface charges within the Debye length produces a measurable electrical signal readout scaling with the concentration of target analytes that can be determined by either using a transducer (e.g., field-effect transistor) or directly measuring the open circuit potential (OCP) between the sensing electrode (SE) and a reference electrode (RE).[34−38] A layer of 6-mercapto-1-hexanol (MCH) occupies the rest of the Au surface, providing passivation to block nonspecific interactions. Figure 2B shows the values of OCP of an aptamer-functionalized commercial gold disk electrode in 1× phosphate-buffered saline (PBS) solutions with different concentrations of cocaine ranging from 10^{-11} to 10^{-5} M (aptamer to MCH ratio = 1:100, sensitivity = −2.89 ± 0.49 mV/dec). The monotonic decrease in OCP values with an increasing concentration of cocaine suggests the reorientation of DNA strands closer to the surface upon the binding event, bringing more negative charges into the electric double layer (EDL).[4] The sensitivity under high ionic strength conditions is particularly advantageous for directly measuring target samples in point-of-care and/or in vivo applications. In contrast, tests in 0.1× PBS (pH = 7.4) (Figure S1) suggest a lower stability and a larger sample-to-sample variation, with an extracted sensitivity of ∼−1.13 ± 0.16 mV/dec. This observation may be due to the reduced stability of secondary structures and binding conformation of aptamers with a decreased number of ions in the environment.[39]Figure 2C and D show results of the electrochemical impedance spectroscopy (EIS) of the functionalized surface in different test solutions. Fitting the Nyquist plots based on a Randles circuit model shown in the inset estimates the charge transfer resistance (R_{ct}) between the redox probes ($[Fe(CN)_6]^{3-/4-}$) and the sensing interface (Table S1), which shows a decreasing trend upon the binding of more cocaine. It is important to note that other competing mechanisms, such as the charge of cocaine in solution and the steric repulsion between aptamers, may also affect the measured results. To this end, systematically varying the ratio of aptamer to MCH provides insight into the structure−property interrelationship. The calibrated response−concentration plots and extracted sensitivities for different sensors appear in Figure 2E and F: the value of sensitivity of devices with a ratio of 1:10, 1:50, 1:100, and 1:150 corresponds to −0.79 ± 0.14, −1.79 ± 0.14, −2.89 ± 0.49, and 0.23 ± 0.25 mV/dec, respectively. The results indicate an optimized sensitivity with the ratio of 1:100, which is consistent with the conclusion of a similar aptamer-based sensing system reported in a previous study.[40,41] The following part of the study exploits this ratio for sensor development.

Measuring responses to nonspecific binding chemicals evaluates the selectivity of this sensing platform. Biomolecules having a considerable concentration in bodily fluids (e.g., glucose, urea, lactate, bolvine serum albumin (BSA)) and a similar chemical structure/molecular weight (e.g., atropine, tropinone)[42] are potential interferents of interest. Additionally, a recent study shows that cocaine can increase endogenous serotonin in the ventral pallidum, and therefore, this study also investigates the cross-sensitivity for potential applications in the future.[43] The chemical structures of the analytes used here and the corresponding response−concentration plots appear in Figure S2, with extracted values of sensitivity shown in Figure 2G. A sensitivity of −2.89 ± 0.49 mV/dec for cocaine in contrast to −0.66 ± 0.07 mV/dec for glucose, −1.51 ± 0.11 mV/dec for atropine (due to the structural similarity), 0.04 ± 0.15 mV/dec for serotonin, 0.37 ± 0.24 mV/dec for tropinone, −1.57 ± 0.26 mV/dec for BSA (due to large molecular weight), and −0.47 ± 0.25 mV/dec for urea suggests a specificity. The mechanism underlying the response for glucose, urea, lactate, BSA, and serotonin might be nonspecific interactions between analytes and the sensor surfaces, whereas that for atropine and tropinone might originate from their interactions with aptamers due to the structural similarity to cocaine. Further optimizations are possible via the proper passivation to minimize nonspecific interaction and adsorption on both the SE and RE.

Regeneration of Anti-Cocaine Sensors Enabled by pH-Induced Allostery. As discussed in the preceding section, the addition of the pH sensitive motif at the 5′ end of the aptamer (denoted as Aptamer 1) can enable the duplex-to-triplex transition in the acidic environment, resulting in the disruption of the stem-loop structure followed by the release of binding ligands. Increasing the pH value of the environment will reverse the conformation by forming a duplex again and thereby recover the function of the aptamers for capturing target ligands. Figure 3A shows the schematic illustration of the regeneration process enabled by allostery upon pH regulation. On the other hand, the DNA strand without the pH sensitive motif (denoted as Aptamer 2) lacks the capability of forming a triplex, and thereby is expected to be insensitive to pH-induced regeneration. Figure 3B shows responses of Au electrodes functionalized with Aptamer 1 to cocaine solutions (1× PBS) with varying concentrations and different pH values (4.0, 5.0, 6.0, and 7.4). The results suggest a decreasing trend in sensitivity as the environment becomes more acidic, which is consistent with the mechanism stated above. Interestingly, studies under the same test conditions but with 0.1× PBS cannot provide stable, monotonic responses in any cases (Figure S1). The observation further supports that the ionic coordination may influence[39,44] the loop topology of the DNA strand and play an important role in stabilizing the anti-cocaine aptamers used in this work.

Treating cocaine-adsorbed devices (after completing measurement in 10^{-5} M cocaine solution samples) with acidic solutions allows for regeneration based on the duplex-to-triplex transition. Systematic studies investigate effects of key parameters of experimental conditions including pH value, treatment time, and agitation. To ensure a similar starting point, only devices showing an initial sensitivity of >2.5 mV/dec (absolute value) are selected for the regeneration study described in the following section. Figure 3C presents the calibrated response−concentration curves of sensors after regeneration in solutions with pH values of 4.0, 5.0, and 6.0 for 60 min. The results show that with a pH value of 5.0 or less, the sensors can restore most of the function, regaining a sensitivity of ∼−3.2 mV/dec on average. When the pH value increases to 6.0, however, used devices do not show observable sensitivity after treatment, indicative of an insufficient level of protonation of the N3 in cytosine for completely transitioning the duplex stem into a triplex containing CGC^+ for efficient ligand dissociation. Figure 3D presents responses of regenerated devices after immersion in solution with a pH of 5.0 for 30, 45, and 60 min. The results demonstrate a trend that increasing the treatment time can promote the restoration of sensitivity, which might correspond to the time needed for the ligand to disrupt noncovalent interactions, dissociate from aptamers, and diffuse away into the bulk solution. Systematic studies with agitation (speed: 150 rpm (rpm)) show a similar

https://doi.org/10.1021/acsnano.2c08511
ACS Nano 2022, 16, 20922−20936

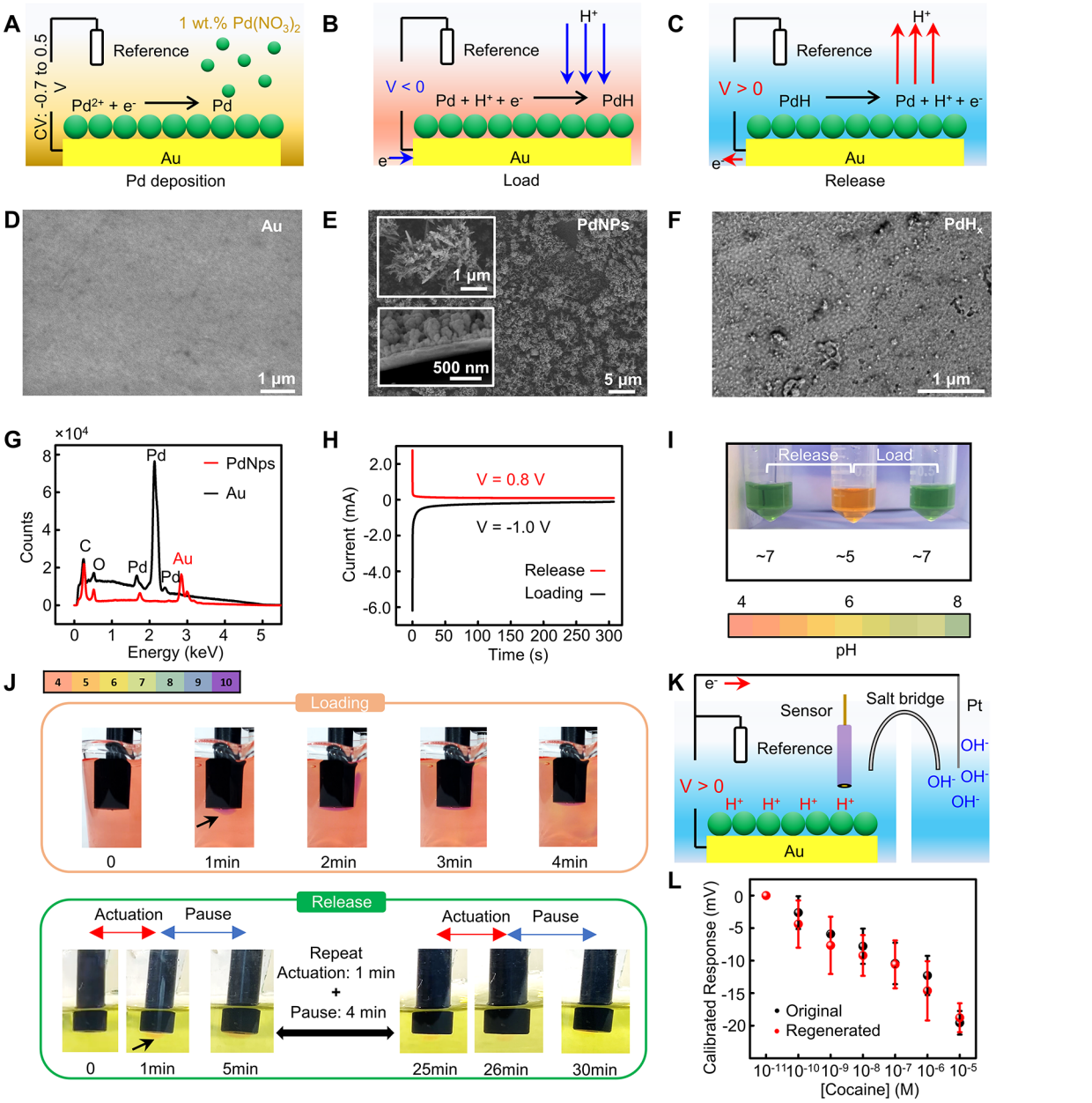

Figure 4. Design, fabrication, and characterization of Pd electrodes for local pH regulation. (A–C) Schematic illustration of preparing Pd electrodes as the pH regulator that can modify the concentration of protons in the surrounding environment via electrochemical actuation. (D, E) SEM images of the Au surface before (D) and after (E) deposition of PdNps (~300 nm). (F) SEM image of PdH_x after the loading of hydrogens. (G) EDS analysis of Au surfaces before/after electrodeposition confirming the formation of PdNps. (H) *I–t* curves recorded during the loading and release of protons into and from the Pd electrode. (I) Photographs showing changes in pH values of solutions collected near the working electrode before/after the loading/release processes. (J) Sequential photographs showing the dynamic pH change and spatial distribution of protons in solution during the loading and cyclic release processes. The arrows indicate the regions that are going through the color change. (K) Schematic illustration of the experimental setup for regeneration of an anti-cocaine sensor using a Pd/PdH electrode under cyclic actuation shown in (J). (L) Calibrated response plots of the original and regenerated anti-cocaine sensors placed near the Pd electrode during the electrochemical actuation process.

trend and a shorter time (~15 min) for full function restoration (Figure S3), suggesting the feasibility of achieving rapid refreshment of sensing interfaces within dynamic biosystems having continuous blood flow and tissue movement. Tests during repetitively applied sensing and regeneration cycles on three individual devices appear in Figure 3E to G, and Figure 3H summarizes the average value of sensitivity as a function of the regeneration cycle. Generally, an observable decrease in sensitivity starts to appear during the fifth regeneration cycle, and the value drops to near 0 during the seventh cycle, which could be attributed to the degradation of surface functional groups over time in the liquid environment. The results presented here suggest the potential of using the regeneratable sensor system enabled by DNA allostery for real-time monitoring, which can provide status updates on an hourly basis.

Another set of experiments explores the regeneration performance of the sensing interface after being saturated in

https://doi.org/10.1021/acsnano.2c08511
ACS Nano 2022, 16, 20922–20936

a higher concentration cocaine solution (up to 10^{-3} M). As shown in Figure S4, the results suggest that a higher concentration can affect the quality of the regenerated sensors: while the calibration plot after regeneration (pH = 5.0, 60 min) does show a similar trend of decrease in OCP values with an increasing cocaine concentration, the extracted sensitivity (-1.79 ± 0.39 mV/dec) is lower than the original one (-2.66 ± 0.78 mV/dec), and the variation among different samples also increases. Two reasons might account for this observation: (1) A highly saturated sensor surface requires a longer regeneration time for the complete dissociation of adsorbed analytes; and (2) the as-purchased cocaine solution used for this study exploits acetonitrile as the solvent, and the higher amount of the organic solvent in a less diluted test solution (10^{-3} M) may cause the degradation of aptamers during the test.

To demonstrate the importance of the pH sensitive motif, control experiments with Aptamer 2 having the same anti-cocaine DNA sequence but without the triplex-forming motif serve as a comparison. The response−concentration curve under the pH neutral condition shows the opposite trend to that of Aptamer 1 with a positive value of sensitivity (2.3 mV/dec). A possible reason for this observation is that Aptamer 2 may go through an opposite conformational change upon the binding of cocaine by reorienting away from the surface, which consequently decreases the number of negative surface charges (as illustrated in Figure 3A). In the meantime, the positive charges cocaine molecules carry[45,46] may also contribute to the increase in surface potential. Interestingly, fitting values (Table S2, Figure S5) of Nyquist plots (Figure 3J) demonstrate the same trend of monotonic decrease as observed for Aptamer 1, consistent with a previous study on EIS sensors for cocaine.[47] The mechanism underlying the response is worth further investigation, which could be due to a combined effect of changes in surface potential, charges of adsorbed analytes, and steric hindrance leading to a decreased electrostatic repulsion of redox probes.[48,49] Due to the lack of pH sensitivity of Aptamer 2, acid-treated sensors (pH = 5.0, treatment time = 60 min) show a very limited capability of regeneration, with an almost negligible sensitivity after the first acid-treatment cycle.

In addition to the example of regeneratable cocaine sensors, it is important to explore the versatility of this technology to other biomolecules. Figure S6 shows the regeneration performance of sensors functionalized with pH sensitive antistreptavidin and antithrombin aptamers and the underlying mechanism based on the allosteric regulation of the DNA sequences: at a neutral pH condition, both aptamers are in a folded conformation for the binding of streptavidin and thrombin molecules with a high affinity.[50,51] Following a very similar working principle to that of the anti-cocaine aptamers, the addition of extra protons in an acidic environment results in a mismatch between the base pair G and A, leading to a disruption of the original conformations and, accordingly, the release of adsorbed analytes for surface regeneration. In both cases, the devices can fully restore the sensitivity after an acid treatment (pH = 5.0) for 60 min (for streptavidin: -3.83 ± 0.78 mV/dec (before) vs -4.44 ± 0.43 mV/dec (after); for thrombin: -3.34 ± 0.91 mV/dec (before) vs -3.42 ± 0.72 mV/dec (after)). The results on alternative biomolecules in addition to cocaine suggest the versatility of this sensing scheme based on allosteric DNAs.

Local pH Regulation with Pd/PdH$_x$ Electrodes via Electrochemical Actuation. To circumvent the challenge of integrating chemical reagents within the sensor chip for regeneration, the study presents a solution by introducing a palladium (Pd)-based bioprotonic pH regulating electrode that can control the pH value of local environments through electrochemical actuation.[52−54] Unlike most metals, which are good contacts for electrons but poor for protons, Pd has a strong affinity to hydrogen and thereby can support the loading/release of protons via the reversible electrochemical reaction: $H^+ + e^- \leftrightarrow H$. The formation of palladium hydride (PdH_x) stores hydrogen, and oxidizing the resulting system can convert hydrogens back to protons again upon the application of a positive voltage, lowering the pH values of the local chemical environment. Schematic illustrations of the fabrication process and working principles for pH control appear in Figure 4A to C. Electrochemical deposition using cyclic voltammetry forms Pd nanoparticles (PdNps) on the surface of a Au electrode (Figure S7). Scanning electron microscope (SEM) images of Au surfaces before/after deposition appear in Figure 4D and E, inset, top. The cross-sectional SEM image (Figure 4E, inset, bottom) of the electrochemically deposited PdNps layer (10 cycles) suggests a thickness of ∼300 nm. The surface becomes smoother after the loading of protons as hydrogen atoms diffuse into the interstitial lattice of Pd (Figure 4F). Figure 4G presents the energy-dispersive X-ray spectroscopy (EDS) analysis of Au surfaces before and after the electrodeposition, confirming the successful deposition of PdNps on the electrode: the atomic percentage of Au on the surface decreases from 23.79% to 0.71%, while Pd increases from 0.04% to 27.13%, respectively (Tables S3 and S4).

Electrochemically loading the PdNp-decorated electrode with protons in an acidic environment followed by release tests in pH neutral solution examines the function of the pH regulator: soaking the electrode in 500 mM NaCl solution (with 0.1 mM H_2SO_4) at pH 4.0 with an applied voltage of -1.0 V for 300 s allows for the adsorption and reduction of H^+ to form PdH_x. Figure S8 shows the current change for an as-prepared electrode (diameter: 2 mm) over time during the loading process and results of integrating current over time. The calculated total amount of proton capacity of the electrode is $\sim 2.39 \times 10^{-7}$ mol (Supplementary Note S1). After that, immersing the electrode loaded with hydrogen in a 500 mM NaCl solution at pH 7.0 with an applied voltage of 0.8 V leads to the oxidation and release of protons (Figure 4H). Collecting solutions (∼400 μL) in the surrounding environment near the electrode during the process and adding a universal pH indicator (Merck, a mixture of thymol blue, methyl red, bromothymol blue, and phenolphthalein, pH transition range: 4.0−10.0) qualitatively visualize the change in pH values (Figure S9 and 4I). Please note that the color difference in Figure S9 is due to the use of different solution samples; that is, the release test on the right does not start with the resulting solution after loading. To better demonstrate the reusability of the electrodes, Figure 4I shows the reversible color change of solutions collected near the working electrode during the repetitive loading/release process, which further supports that the pH regulating electrode is reusable.

Taking sequential photographs during the loading/release processes with the pH indicator evaluates the concentration gradient of protons at the sensor−solution interface as a function of time by capturing the color change (Figure 4J). The actual amount of solution going through the pH change depends on the dimension of the electrode (diameter: 3 cm for

https://doi.org/10.1021/acsnano.2c08511
ACS Nano 2022, 16, 20922−20936

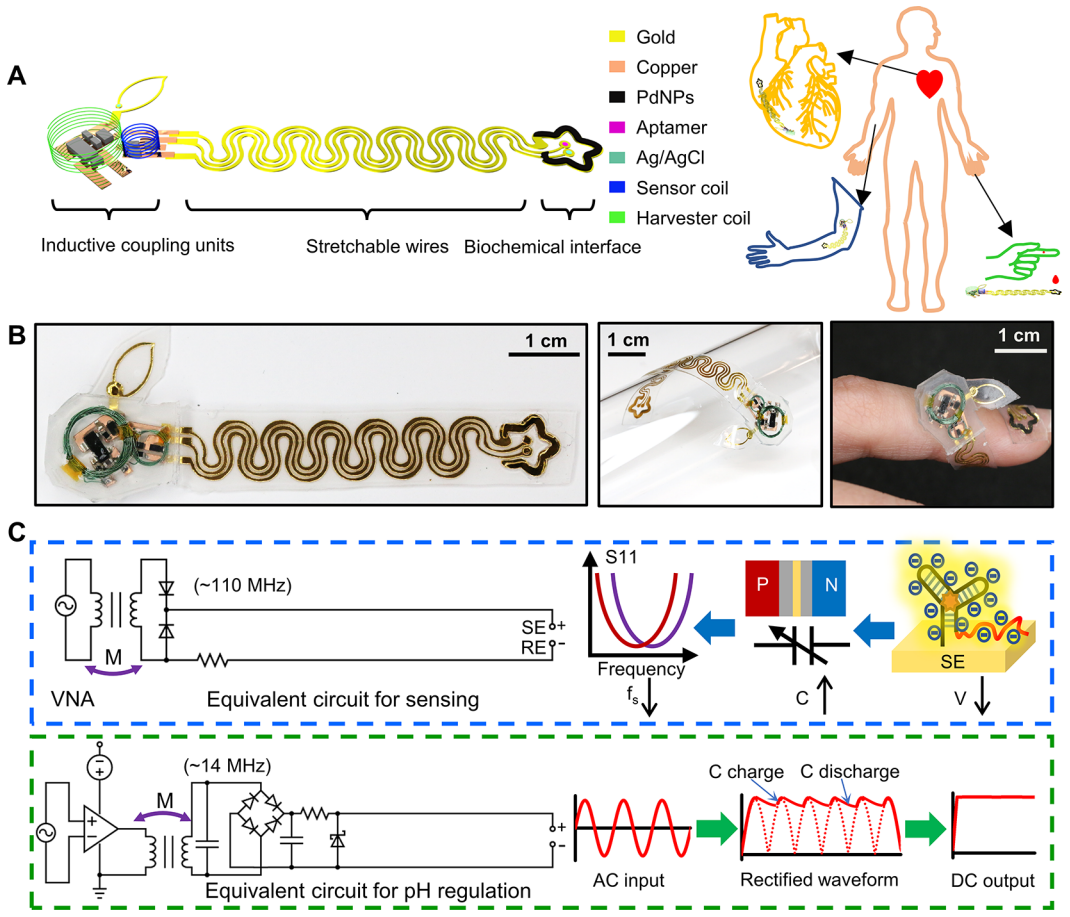

Figure 5. Design of biointegrated electronic systems with wireless sensing/electrochemical actuation capabilities based on the regeneration scheme described in this work. (A) Schematic illustration of a "flower-shaped" sensor prototype integrated with an inductive coupling unit for wireless data transmission and RF energy harvesting, and envisioned applications of the bioelectronics (i.e., as wearable, implantable, and point-of-care devices). (B) Photographs of a wireless device in flat and bent configurations. (C) Equivalent circuits and flowcharts for the signal and power conversion−transmission processes during wireless operation of the device through inductive coupling.

Figure 4I and 2 mm for Figure 4J). The purpose of using Figure 4J is to show that the loading and release processes only modify the local chemical environment near the electrode surface (as indicated by the arrows), while the pH for the rest of the bulk solution can remain unchanged.The loading increases the pH value of the environment, and the system reaches equilibrium within ∼5 min. As discussed earlier, while the conformational switch of aptamers usually takes place rapidly in response to pH regulation, the time needed for the dissociation of substrates from the aptamers represents the bottleneck for sensor regeneration. Consequently, it is important to maintain an acidic chemical environment over a prolonged period (i.e., at least 10−20 min, according to results in Figure S3). Since a sudden release of all protons in the electrode may create an overconcentrated acid environment, the study exploits a cyclic electrochemical actuation protocol with an application of voltage for 1 min followed by a pause for 4 min to fully make use of the loaded protons and to provide a relatively mild condition for potential applications in biosystems. As shown in the sequential photographs, the concentration gradient can remain at the sensor surface after 6 cycles (30 min). Placing a cocaine-adsorbed Au electrode close to an as-prepared pH regulating electrode and conducting the cyclic actuation validate the regeneration scheme (Figure 4K). To ensure high efficiency of regeneration, the study separates the working and counter electrodes using a salt bridge, as the reduction reaction occurs simultaneously at the counter electrode, resulting in an increase in local pH values. Figure 4L shows the response plots of the original and regenerated sensors with a sensitivity of −3.26 and −3.13 mV/dec, respectively. The negligible difference suggests the feasibility of using this scheme for restoring the sensing capability of allosteric DNA-functionalized sensors.

Design and Characterization of Biointegrated, Wireless Electronic Systems. The platform combining the allosteric aptamer functionalized interface and the pH regulator offers a route to developing reusable biosensors. In addition to the biochemical interfaces, for health monitoring purposes, it is also important to design matching coupling strategies for the transmission of sensing data and powering of the pH regulating electrode, ideally, in a wireless manner. To address this issue, the study presents a regeneratable "flower-shaped" sensor prototype for wireless sensing and electrochemical actuation. Figure 5A, left, shows the schematic illustration of a stretchable "flower-shaped" device based on the circuit model. The device consists of three key functional parts: (1) "petals": a biochemical interface with a pair of SE and RE surrounded by a PdNps-decorated metal trace, (2) "leaf": an inductive coupling unit with one coil for data transmission and another coil for RF energy harvesting and electrochemical actuation, and (3) "stem": stretchable wires connecting parts (1) and (2). Patterning the wires into serpentine structures

https://doi.org/10.1021/acsnano.2c08511
ACS Nano 2022, 16, 20922−20936

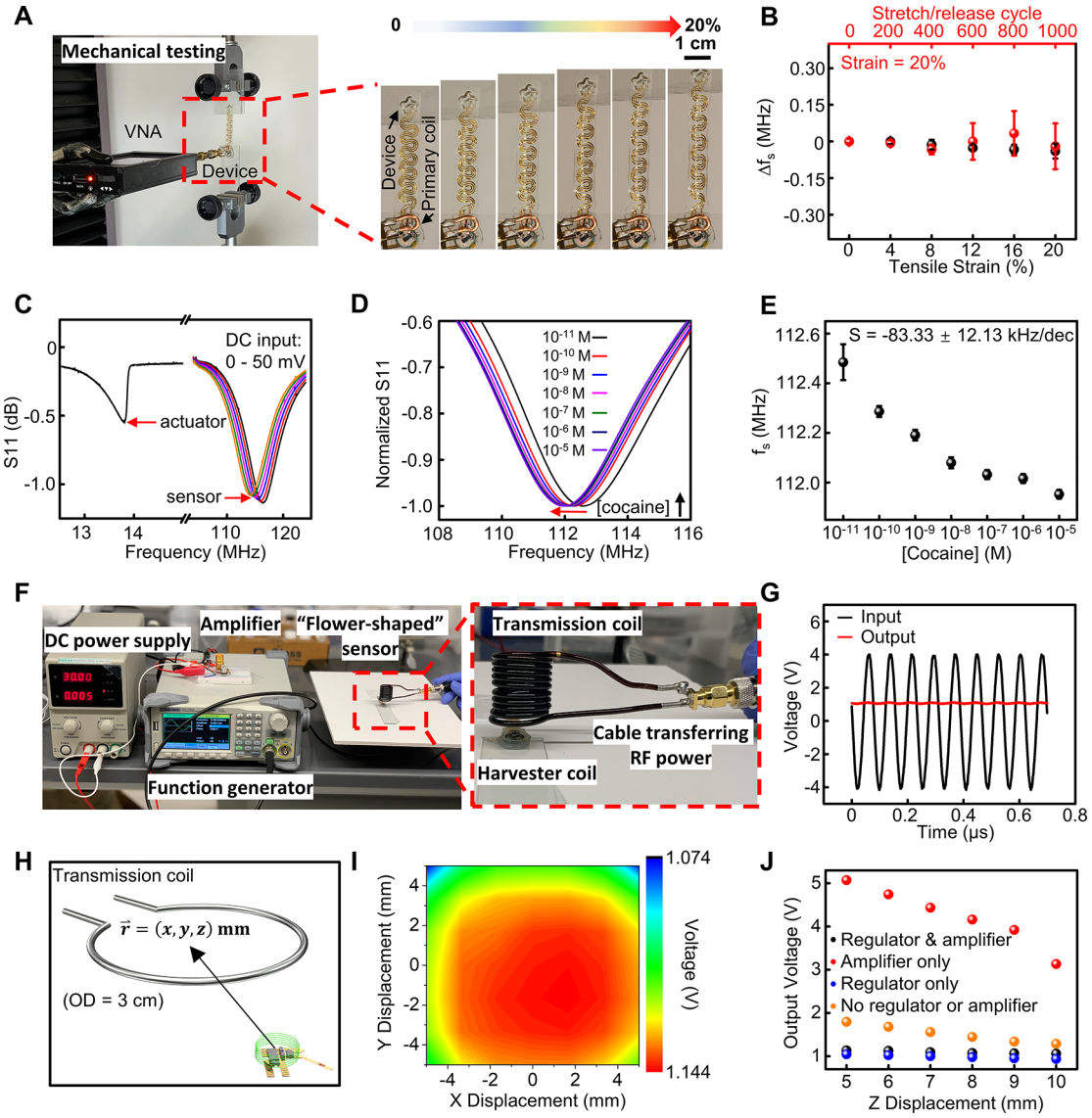

Figure 6. Characterization of the "flower-shaped" wireless electronic device. (A) Experimental setup for the cyclic stretch/release test using a tensile tester, and photographs of a device with a tensile strain ranging from 0 to 20% applied to the stretchable "stem". (B) Change in f_s of the sensor coil as a function of the applied tensile strain and stretch/release cycles. (C) Resonance curves of the coils for the sensor and pH regulator showing distinct values of f_s achieved via proper design of the coil structures. The value of f_s of the sensor coil becomes larger with an increasing input DC voltage serving as the reverse bias for diodes in the circuit. (D) Normalized values of measured S11 of an anti-cocaine sensor functionalized with the pH sensitive aptamer. (E) Extracted value of f_s in D as a function of cocaine concentration. (F) Experimental setup of the wireless electrochemical actuation system. (G) An RF energy radiated from the transmitter by applying an alternating current (sine wave) and the resultant output DC voltage signals wirelessly collected by the harvester (after rectification and voltage regulation). (H) Schematic illustration of the relative position between the harvester and transmitter coils. (I) Mapping of measured output voltages as a function of lateral displacement of the transmission coil from the origin (z = 5 mm). (J) Recorded output voltage as a function of displacement of the transmission coil along the z-axis with and without the Zener voltage regulator and amplifier ($x = y$ = 0 mm).

enables the distribution of mechanical strains and protections of functional parts from deformation when integrated with biotissues. This modularized device also allows for the physically separated placement of parts (1) and (2) to provide seamless integration with target biotissues/biofluids and efficient, stable coupling with external electronics. Figure 5A, right, shows envisioned applications based on the sensor prototype, including using custom-designed devices as wearable, implantable, and point-of-care systems. The benefit of having a cocaine sensor wireless and stretchable is to enable the transmission of sensing data and powering of the pH regulating electrode in a biointegrated manner for continuous monitoring of drug levels within the human body. For wearable electronics, this sensing platform can be worn on different locations such as the forehead, arm, back, and so on, whereas the functional sensing/actuation part can extend to places of interest with biofluids. Figure 5B demonstrates photographs of the "flower-shaped" device in flat and bent configurations highlighting its flexibility.

The equivalent circuit diagrams for the sensor and actuator are in Figure 5C. For the biochemical sensing circuit, the surface potential change caused by analyte−aptamer interaction serves as a reverse bias for a pair of varactor diodes, which modifies the thickness of the depletion region in the p−

https://doi.org/10.1021/acsnano.2c08511
ACS Nano 2022, 16, 20922−20936

n junction in the diodes. The modification leads to a change in capacitance in an inductor−capacitor resonance circuit and shifts the resonance frequency according to the following equation:

$$f_s = \frac{1}{2\pi\sqrt{LC}}$$

where L and C are the inductance and capacitance of the circuit, respectively. Aligning the coupling unit with a readout coil connected with a vector network analyzer and sweeping the frequency record the input return loss (S11), and fitting the curve determines f_s for the quantitative analysis of surface potential change scaling with the change in concentration of cocaine. The pH regulating circuit consists of a Pd-coated metal trace surrounding the sensing site and an inductive coupling unit which can wirelessly capture RF power in the range of 13−14 MHz (transmitting frequency = 13.3 MHz, which falls into this range to ensure maximized energy harvesting efficiency) delivered through a vertically aligned transmission antenna. A full-wave bridge rectifier (for AC to DC conversion), a smoothing capacitor (for evening out fluctuations), and a Zener diode regulator (490 ohm, for voltage stabilization) then convert the harvested energy into a DC voltage (∼1.1 V) that can support the release of preloaded protons for localized pH modulation. Placing the counter electrode away from the sensing area minimizes the effect of the reduction reaction, increasing the local pH around it, which may suppress the efficient aptamer regeneration. Details about the design, operation, and characterization appear in the following section.

Preparing the metal traces for the three key parts using a simple "cut-and-paste" method followed by soldering electronic components and connecting them with silver epoxy yields the resulting flexible electronic system. The low modulus and high elasticity of the device can significantly reduce the probability of mechanical failure when serving as biointegrated electronics. Cyclic stretching tests evaluate the mechanical robustness of the system. Figure 6A shows photographs of a test device subject to a strain of up to ∼20%, which encompasses the elastic stretchability of the epidermis (∼15%).[55] Here incorporating a damping resistor (10 Kohm) in series with the SE and RE isolates the DC circuitry from the coupling unit and minimizes variations in f_s due to changes in parasitic inductance/capacitance resulting from mechanical deformation. Figures 6B and S10 show f_s with varied tensile strains and before/after a different number (0−1000) of stretch/release cycles. The value of f_s remains largely unchanged throughout the test with little dependence on the tensile strain, highlighting the potential of the system serving as biointegrated electronics on nonflat surfaces with external strains.

A rational design of the wireless sensor and actuator separates their operational frequencies for individual functions. Additionally, increasing the number of coil turns of the coupling unit for the actuator leads to a larger magnetic flux as the power supply for pH modulation. This study uses a 5-turn (diameter: 3 mm) and a 20-turn (diameter: 5 mm) coil for the sensor and actuator, and the resonance curves appear in Figure 6C with an f_s of ∼115 and 14 MHz, respectively. Applying a reverse bias voltage ranging from 0 to 30 mV across the SE and RE and recording the resonance frequency with an external antenna connected to a portable vector network analyzer (NanoVNA) placed on the top examine the performance of the circuit in transmitting static DC input simulating surface potentials associated with the potentiometric sensor design. f_s of the coupling unit shifts to larger values with an increasing bias based on the voltage frequency modulation working principle described in the preceding section, yielding a voltage sensitivity of 0.042 MHz/mV. Following this principle, connecting the functionalized electrode pairs to the wireless circuit (SE with cathode, and RE with anode) forms a sensing system capable of detecting the concentration of cocaine. Exposing the sensor part to cocaine solutions with varying concentrations results in a shift in f_s due to modification in surface potential (Figures 6D and S11). Figure 6E shows the extracted f_s as a function of cocaine concentration, with a sensitivity of −83.33 ± 12.13 kHz/dec The above results demonstrate that the platform possesses sufficient voltage sensitivity for wireless chemical sensing.

Beyond the sensing capability, magnetic resonance coupling serves as a simple, straightforward, and competing technique for powering wireless bioelectronics due to the resistance to environmental interference.[31,56−60] Additionally, separating the energy harvester from the PdNp-functionalized interface matches the design of the modularized sensor system. The "two-part" design provides opportunities for building bio-integrated electronics with advanced functions and improved stability in performance. To evaluate the performance in power transfer, systematic studies investigate the effect of relative position change between the transmitter (OD = 3 cm) (connected to a function generator and a power amplifier) and receiver (connected to an electrochemical workstation) in three directions along a vector (starting and end points: the center of the harvester and transmission coils, respectively) (Figure 6H). The setup of the experiment appears in Figure 6F: a function generator ($V_{AC,\,sin} \approx 10\ V_{pp}$, transmitting frequency = 13.3 MHz) supplies a continuous RF energy followed by power amplification. The inductive coupling between the transmitter and receiver delivers the RF electrical power to the electrochemical actuation system followed by waveform rectification and voltage regulation. Figure 6G illustrates the amplified waveform wirelessly supplied to the transmitter coil (measured across the output ports of the cable after power amplification) and the harvested DC voltage measured across a load resistor (10 Kohm, determined based on the EIS spectrum of a PBS solution, Figure S12) connected to the interface for pH modulation. The frequency separation and the lateral displacement between the coupling units for the sensor and actuator prevent unexpected activation of nontarget components. Figure 6I shows a mapping of the output voltage corresponding to relative position displacement in (x, y) from (−5, −5) mm to (5, 5) mm, with z = 5 mm (raw data in Figure S13). The output voltage remains highly stable throughout the test ranging from 1.074 to 1.144 V, which meets the requirement of Pd/PdH_x electrodes for the oxidation reaction. Similarly, Figure 6J shows the results with (x, y) fixed at (0, 0) and a varying distance along the z-axis. For the two control groups without the voltage regulator (red and orange), the difference in voltage output at the same position (>2 times) suggests the importance of the power amplifier to ensure a sufficient supply of energy for the electrochemical actuation. The results without the voltage regulator also demonstrate a considerable variation in output voltage signals throughout the measurement range. On the contrary, adding the voltage regulator minimizes displacement-associated variation in voltage, providing an enhanced stability for controlled

https://doi.org/10.1021/acsnano.2c08511
ACS Nano 2022, 16, 20922−20936

electrochemical actuation. Overall, the characterizations of wireless sensing and RF energy harvesting suggest the potential application of the inductively coupled electronic system in facilitating closed-loop biomarker detection and in vivo regeneration when combined with a properly designed sensing interface and pH regulating materials.

Figure S14 shows the regeneration performance of a packaged "flower-shaped" stretchable wireless device with on-chip serpentine wires, aptamers, and PdNps. Details about the connection between the inductive coupling unit and the SE/RE pairs based on their polarity appear in Figure S14A. Figure S14B and C present the resonance curves showing the shifts in f_s due to the changes in the cocaine concentration before and after the regeneration process enabled by the pH regulator (following the actuation protocols in Figure 4J). Figure S14D and E summarize the extracted f_s as a function of cocaine concentration, and Figure S14F presents the calibrated OCP response calculated based on data in Figure S14D and E (before: -2.55 ± 0.74 mV/dec, after: -2.86 ± 0.31 mV/dec). The results demonstrate the functionality and reusability of the packaged system, further highlighting the mechanical stability and energy harvesting capability of the stretchable device.

CONCLUSIONS

In summary, the results presented in this study describe an interface design strategy with allosteric DNA as bioreceptors and an associated integration scheme for building regenerat-able biochemical sensors. The resulting system combines LC resonance circuits, a stretchable design, a Pd-based bioprotonic pH regulator, and an anti-cocaine aptamer-based biosensing interface. As a case study, a re-engineered anti-cocaine aptamer with a pH sensitive domain can regain its affinity with target analytes due to proton-promoted duplex-to-triplex transition in DNA configuration followed by the release of adsorbed ligands. Sensitivity studies using aptamer-functionalized Au surfaces suggest the capability of this platform in measuring cocaine concentrations across a wide concentration range (10^{-11} to 10^{-5} M) via a potentiometric sensing strategy. Systematic studies verify the reusability of this anti-cocaine aptamer upon proper treatment in acidic environments. Additionally, placing a Pd/PdH_x electrode and releasing protons via electrochemical reactions allow for the pH regulation of the local chemical environment. Demonstration of a "flower-shaped", stretchable, and inductively coupled electronic systems with sensing and energy harvesting capabilities provides a promising route to designing wireless devices in biointegrated forms customizable for multiple application scenarios. Although the current study focuses on cocaine sensing as a proof-of-concept, when combined with other types of SELEX-enabled allosteric DNAs, the resulting system can readily extend to alternative biomarkers. Overall, this study sets the stage for developing promising engineering tools for continuous monitoring of biological markers through seamless and stable integration with target biosystems.

METHODS

Materials and Reagents Used for This Study. PBS, Tris-EDTA buffer solution (TE), cocaine solution ($C_{17}H_{21}NO_4$, 1.0 mg/mL in acetonitrile, ≥99%), glucose (D-glucose, ≥99%), atropine ($C_{17}H_{23}NO_3$, 1.0 mg/mL in acetonitrile), 5-hydroxytryptamine, 3-(2-aminoethyl)-5-hydroxyindole, 5-HT (serotonin hydrochloride), streptavidin, thrombin (citrate-free, human serum), tropinone (99%), BSA, urea, MCH, DL-dithiothreitol (DTT, ≥99%), hydrochloric acid (HCl), palladium(II) nitrate ($Pd(NO_3)_2$) solution (99.999%, 10 WT), universal indicator solution (pH 4.0 to 10.0), potassium hexacyanoferrate(III) ($K_3[Fe(CN)_6]$), and potassium hexacyanoferrate(II) trihydrate ($K_4[Fe(CN)_6]\cdot 3H_2O$) were purchased from Sigma-Aldrich. Single-stranded DNA aptamers were synthesized by and purchased from Integrated DNA Technologies and Biosearch Technologies Inc.

Fluorescence Intensity Characterization. The anti-cocaine aptamer sequence with the pH sensitive motif, fluorophore (ATTO488) and quencher (BHQ-1), was synthesized by Biosearch Technologies Inc. (5′-(ATTO488)CCC TCT ATT TCT CTC CCT TT(BHQ-1)GGG AGA CAA GGA AAA TCC TTC AAT GAA GTG GGT CGA CA-3′). Dissolving the aptamers in PBS solution (100 μM) with different pH (4.0, 5.0, 6.0, and 7.4) and mixing the resulting systems with 2×10^{-11} M cocaine solution in 1:1 ratio formed a series of test solutions. Injecting the test solutions into a 96-well plate finished the preparation of samples. The characterization of fluorescence intensity took place with a SpectraMax M5 plate reader at 25 °C. The study used an excitation wavelength of ∼488 nm and measured the emission spectrum in the wavelength ranging from 530 to 550 nm. Gradually adding a cocaine solution (from 10^{-11} to 10^{-3} M) into the wells enabled the characterization of fluorescence emission of the pH sensitive aptamer in the presence of the substrate with varying concentrations.

Preparation of Aptamer-Modified Au Electrode Surfaces. Thiolated anti-cocaine aptamers (with pH sensitive motif: 5′-CCC TCT ATT TCT CTC CCT TTG GGA GAC AAG GAA AAT CCT TCA ATG AAG TGG GTC GAC A/3Thio-MC3-D/-3′; without pH sensitive motif: 5′-GGG AGA CAA GGA AAA TCC TTC AAT GAA GTG GGT CGA CA/3Thio-MC3-D/-3′), thiolated antithrombin aptamers (5′-GGT TGG TGT GGT TGG CTC TAA AAA AAA AAA AAA A/3Thio-MC3-D/-3′), and thiolated antistreptavidin aptamers (5′-ATA CCA GCT TAT TCA ATT ATT GAC CGC TGT GTG ACG CAA CAC TCA ATT CTT GGA TCT CGC TGC ACA CAG ATA GTA AGT GCA ATC T/3Thio-MC3-D/-3′) were synthesized by Integrated DNA Technologies based on sequences reported in previous studies.[29,50,51] Dissolving as-purchased aptamers in 1× TE solution with 10 mM DTT reduced the disulfide bonds and yielded a solution of aptamers with −SH groups at the 3′ end (concentration: 100 μM). Centrifuging the resulting solution in a MySpin12 (Thermo Fisher Scientific) at 2038 relative centrifugal force (RCF) (2600 rpm) for 4 min removed additional DTT. Mixing the purified aptamer solution with 10 mM MCH solution in TE buffer (v/v ratio: 1:1) formed the coating solution for functionalizing Au surfaces. Heating the mixture in a water bath at 95 °C for 5 min converted the DNA strands in solution to a fully extended conformation, and a subsequent rapid cooling step in an ice bath for 15 min stabilized the resulting structure. Drop-casting the solution on a Au electrode surface (commercial gold disk electrode or thin-film Au deposited by electron-beam evaporation) and drying the system overnight at room temperature completed the immobilization of aptamers by forming Au−S bonds at the 3′ end, with MCH serving as the passivation layer blocking the rest of the Au surface. Storing functionalized electrodes in 1× PBS solution at 5 °C retained the activity of aptamers for use over an extended period.

Preparation of Cocaine Solutions. Diluting a cocaine acetonitrile solution (1.0 mg/mL) with 1× PBS (pH 7.4) formed a set of test solutions with varying concentrations ranging from 10^{-11} to 10^{-4} M. Similarly, dissolving atropine, glucose, serotonin, and other interferents in 1× PBS yielded corresponding test solutions. For the study on the effect of pH values, adding 1 M HCl to cocaine solutions modulated pH values of the systems to 4.0, 5.0, and 6.0. For the study on the effect of ionic strength, diluting the systems with deionized (DI) water formed test solutions in 0.1× PBS.

Electrical Characterization of Aptamer-Functionalized Au Electrode. Before each test, incubating the SE in the target solution for 20 min allowed for the system to equilibrate. An electrochemical workstation measured the open circuit potential of the SE vs a Ag/AgCl RE with a sampling rate of 10 Hz. The characterization of electrochemical impedance spectroscopy exploited a three-electrode

https://doi.org/10.1021/acsnano.2c08511
ACS Nano 2022, 16, 20922−20936

setup with Ag/AgCl as the RE, a Pt wire as the counter electrode, and $K_4Fe(CN)_6/K_3Fe(CN)_6$ (1:1) (1 mM for both) as the redox couples. All measurements in this study took place at room temperature.

Deposition of Pd Nanoparticles for pH Regulation. Treating a Au electrode using cyclic voltammetry (from −0.7 to 0.5 V vs Ag/AgCl) in 1 wt % $Pd(NO_3)_2$ for 10 cycles deposited a layer of Pd nanoparticles on the surface.[53,54] Loading PdNps in an acidic solution (pH = 4.0) with an applied voltage of −1.0 V for 200 s converted the surface to PdH_x. Placing the Pd/PdH_x electrode into a pH-neutral solution and applying a positive voltage of 0.8 V enabled the release of protons. A pH indicator (50 μL per 1 mL solution) visualized the pH gradient at the solution−electrode interface, and a camera recorded the dynamic change of the gradient as a function of time.

Characterization of Deposited PdNps. A Thermo Scientific Apreo FEG SEM characterized the surface morphology of bare gold film and gold film deposited with PdNps before and after the load of hydrogen (acceleration voltage: 5 kV). EDS analyzed the elemental composition of the surface before and after deposition of PdNps.

Fabrication of Stretchable "Flower-Shaped" Sensing/Actuation System. The patterning of metal traces of the electronic device followed a cut-and-paste method reported in previous studies.[61] The process began with laminating a conductive copper tape (Amazon, for the inductive coupling unit) or a polyimide (PI) (HD MicroSystems) film (thickness: (~13 μm) with 300 nm Au onto an ultraviolet (UV) light dicing tape (Shenzhen You-San Technology Co.). Cutting through the conductive film with a vinyl cutter (Silhouette Cameo 4), exposing the system to UV light, and peeling off unneeded parts created patterned metal traces. Binding the top side of the patterns to a Dragon Skin (Smooth-On) substrate and peeling off the UV releasable tape completed the transfer of the conductive traces. Laminating another layer of Dragon Skin encapsulated the whole system after the soldering of all the electronic components.

Silver epoxy paste electrically connected the copper tape and the stretchable Au serpentine wires. Manually wrapping coils and soldering electronic components to the patterned copper traces according to the circuit diagram completed the fabrication of this stretchable electronic system. This study used the following electronic components assembled as shown in Figure S15: a pair of varactor diodes (SMV1249) and a damping resistor (10 Kohm) for the sensor (coil diameter: 3 mm, 5 turns); two capacitors (15 pF connected to coil and 1 μF connected to bridge rectifier), a bridge rectifier (BAS3007A-RPP), a Zener diode voltage regulator (CMOZ1L8), and a resistor (490 ohm) for the electrochemical actuator (coil diameter: 5 mm, 20 turns).

Preparation of Thin-Film Ag/AgCl RE. Drop-casting a mixture of silver epoxy and hardener (Chemtronic CW2400), curing at room temperature for 12 h, and transforming the surface into AgCl by treating it with sodium hypochlorite solution (5 wt %) for 30 min formed the thin-film Ag/AgCl RE. Meanwhile, preparation of recrystallized KCl(aq) in cold isopropyl alcohol (IPA) yielded ultrafine microsize powders. Dissolving 438 mg of polyvinyl butyral (PVB, 10 wt %) in 5 mL of anhydrous ethanol, mixing the solution with 250 mg of KCl powder, and homogenizing the system in an ultrasonic bath for 10 min yielded an electrolyte cocktail (stored at 7 °C). Drop-casting the cocktail on the Ag/AgCl electrode followed by drying overnight completed the fabrication of the RE.

Characterization of Wireless Electronic System. The reader electronics used for the characterization of resonance frequency consisted of a NanoVNA with a single-turn primary coil (diameter: 3 mm) connected through a Sub-Miniature Version A (SMA) connector. Vertically aligning the primary coil with the electromagnetic coupling unit and sweeping the frequency range obtained the real and imaginary parts of the reflection coefficient (S11) with a dip in the resonance curve around f_s. Fitting the curve determined the value f_s for quantitative analysis.

To characterize the actuation system, an incident RF power was provided by a function generator (Agilent) ($V_{AC,\ sin} \approx 10\ V_{pp}$, transmitting frequency = 13.3 MHz) and enlarged by an amplifier (V_{bias} = 0 V, V_d = 30 V). The RF power is transmitted wirelessly through a transmitter (10 turns, diameter = 3 cm) to the receiver with a vertical distance of 5 mm. According to the EIS characterization of the Pd electrode (Figure S12), a load resistor (10 Kohm) was connected at the output port of the actuator, and the voltage between the load resistor was recorded with an electrochemical workstation.

Mechanical Test. A tensile test system (Instron) was utilized to evaluate the mechanical properties of the wireless system. Shorting the cathode and anode stabilized the varactors in the magnetic coupling unit and minimized environmental noises. f_s of the sensing system was monitored with an applied tensile strain ranging from 0 to 20%. For the cyclic stretching test, the f_s was monitored before and after 0−1000 stretching cycles with an applied tensile strain of 20%.

Statistical Analysis. For measurement of the OCP response of the potentiometric sensors, data were calibrated by using the reading of OCP vs RE in solutions with the lowest concentration of cocaine (10^{-11} M) as the baseline (i.e., calibrated response = 0 mV) to mitigate device-to-device variation. Data were expressed as mean ± standard deviation (SD). The sample size (n) for each statistical analysis was 3 except for those in Figures 3E,F,G and S14.

ASSOCIATED CONTENT

Supporting Information

The Supporting Information is available free of charge at https://pubs.acs.org/doi/10.1021/acsnano.2c08511.

Calibrated response of the anti-cocaine sensors in 0.1× PBS, values of R_s, R_{ct}, and Q (= $P1n1$) for aptamers with and without a pH sensitive motif, extended data for the selectivity study, regeneration behavior of anti-cocaine sensor in 1× PBS solution (pH = 5.0) with different times of agitation, regeneration behavior of anti-cocaine sensor in 1× PBS solution with cocaine concentration up to 10^{-3} M (pH = 5.0, 60 min), extracted charge transfer resistance based on results in Figure 3J, regeneration performance of pH sensitive anti-streptavidin and anti-thrombin aptamer-based sensor, cyclic voltammetry curves during the electrodeposition of PdNps, EDS elemental analysis table of Au film before and after PdNps deposition, quantification of hydrogen capacity in a Pd electrode, calculation of hydrogen capacity of a Pd electrode, change in pH value of solution near the working electrode before/after the loading/release processes, raw data of measured S11 of an anti-cocaine sensor during mechanical testing, raw data of measured S11 of the anti-cocaine sensor in Figure 6D, EIS characterization of the Pd electrode in 1× PBS solution, $V-t$ plots of DC output varying the relative position between the transmission and harvester coils, regeneration performance of a packaged "flower-shaped" wireless device, Autocad design of the inductive coupling units of the "flower-shaped" device (PDF)

Video showing real-time fluorescence emission intensity captured by a fluorescence microscope (MP4)

AUTHOR INFORMATION

Corresponding Author

Jinghua Li − *Department of Materials Science and Engineering and Chronic Brain Injury Program, The Ohio State University, Columbus, Ohio 43210, United States;* orcid.org/0000-0001-8985-566X; Email: li.11017@osu.edu

https://doi.org/10.1021/acsnano.2c08511
ACS Nano 2022, 16, 20922−20936

Authors

Shulin Chen − *Department of Materials Science and Engineering, The Ohio State University, Columbus, Ohio 43210, United States;* orcid.org/0000-0002-0280-1536

Tzu-Li Liu − *Department of Materials Science and Engineering, The Ohio State University, Columbus, Ohio 43210, United States*

Yan Dong − *Department of Materials Science and Engineering, The Ohio State University, Columbus, Ohio 43210, United States*

Complete contact information is available at: https://pubs.acs.org/10.1021/acsnano.2c08511

Author Contributions

S.C. and T.-L.L. contributed equally to this work.

Author Contributions

The manuscript was written through contributions of all authors. All authors have given approval to the final version of the manuscript.

Funding

This work was supported by The Ohio State University start-up funds, the Chronic Brain Injury Pilot Award Program at The Ohio State University, the Ohio State University Center for Medical and Engineering Innovation pilot grant, and the National Center for Advancing Translational Sciences (award number: UL1TR002733). The content is solely the responsibility of the authors and does not necessarily represent the official views of the National Center for Advancing Translational Sciences or the National Institutes of Health. This work was also supported by the Ohio State University Materials Research Seed Grant Program, funded by the Center for Emergent Materials; NSF-MRSEC, grant DMR-2011876; the Center for Exploration of Novel Complex Materials; and the Institute for Materials Research. J.L. acknowledges the support from NSF award ECCS-2223387.

Notes

The authors declare the following competing financial interest(s): T.-L.L. and J.L. are inventors on a pending patent filed by The Ohio State University (application no.: 63/171,694, filed on 7 April 2021). S.C, T.-L.L., and J.L. are inventors on a pending patent filed by The Ohio State University (application no.: 63/359,734, filed on 8 July 2022).

ACKNOWLEDGMENTS

The authors thank The Ohio State University Nanotech West Lab for the facilities regarding device fabrication and characterization.

REFERENCES

(1) Koh, A.; Kang, D.; Xue, Y.; Lee, S.; Pielak, R. M.; Kim, J.; Hwang, T.; Min, S.; Banks, A.; Bastien, P.; Manco, M. C.; Wang, L.; Ammann, K. R.; Jang, K.; Won, P.; Han, S.; Ghaffari, R.; Paik, Ungyu.; Slepian, M. J.; Balooch, G.; Huang, Y.; Rogers, J. A. A Soft, Wearable Microfluidic Device for the Capture, Storage, and Colorimetric Sensing of Sweat. *Sci. Transl. Med.* **2016**, *8* (366), 366ra165.

(2) Li, J.; Liu, Y.; Yuan, L.; Zhang, B.; Bishop, E. S.; Wang, K.; Tang, J.; Zheng, Y. Q.; Xu, W.; Niu, S.; Beker, L.; Li, T. L.; Chen, G.; Diyaolu, M.; Thomas, A. L.; Mottini, V.; Tok, J. B. H.; Dunn, J. C. Y.; Cui, B.; Pasca, S. P.; Cui, Y.; Habtezion, A.; Chen, X.; Bao, Z. A Tissue-like Neurotransmitter Sensor for the Brain and Gut. *Nature* **2022**, *606* (7912), 94−101.

(3) Torrente-Rodríguez, R. M.; Tu, J.; Yang, Y.; Min, J.; Wang, M.; Song, Y.; Yu, Y.; Xu, C.; Ye, C.; IsHak, W. W.; Gao, W. Investigation of Cortisol Dynamics in Human Sweat Using A Graphene-based Wireless mHealth System. *Matter* **2020**, *2* (4), 921−937.

(4) Nakatsuka, N.; Yang, K. A.; Abendroth, J. M.; Cheung, K. M.; Xu, X.; Yang, H.; Zhao, C.; Zhu, B.; Rim, Y. S.; Yang, Y.; Weiss, P. S.; Stojanovic, M. N.; Andrews, A. M. Aptamer-field-effect Transistors Overcome Debye Length Limitations for Small-Molecule Sensing. *Science* **2018**, *362* (6412), 319−324.

(5) Liang, J.; Liu, H.; Huang, C.; Yao, C.; Fu, Q.; Li, X.; Cao, D.; Luo, Z.; Tang, Y. Aggregated Silver Nanoparticles-Based Surface-Enhanced Raman Scattering Enzyme-Linked Immunosorbent Assay for Ultrasensitive Detection of Protein Biomarkers and Small Molecules. *Anal. Chem.* **2015**, *87* (11), 5790−5796.

(6) Li, J.; Peng, Y.; Liu, Y.; Li, W.; Jin, Y.; Tang, Z.; Duan, Y. Investigation of Potential Breath Biomarkers for the Early Diagnosis of Breast Cancer Using Gas Chromatography-Mass Spectrometry. *Clin. Chim. Acta* **2014**, *436*, 59−67.

(7) Zeng, J.; Yin, P.; Tan, Y.; Dong, L.; Hu, C.; Huang, Q.; Lu, X.; Wang, H.; Xu, G. Metabolomics Study of Hepatocellular Carcinoma: Discovery and Validation of Serum Potential Biomarkers by Using Capillary Electrophoresis-Mass Spectrometry. *J. Proteome Res.* **2014**, *13* (7), 3420−3431.

(8) Khansili, N.; Rattu, G.; Krishna, P. M. Label-free Optical Biosensors for Food and Biological Sensor Applications. *Sens. Actuators B Chem.* **2018**, *265*, 35−49.

(9) Aleman, J.; Kilic, T.; Mille, L. S.; Shin, S. R.; Zhang, Y. S. Microfluidic Integration of Regeneratable Electrochemical Affinity-Based Biosensors for Continual Monitoring of Organ-On-A-Chip Devices. *Nat. Protoc.* **2021**, *16* (5), 2564−2593.

(10) Wang, Z.; Hao, Z.; Wang, X.; Huang, C.; Lin, Q.; Zhao, X.; Pan, Y. A Flexible and Regenerative Aptameric Graphene−Nafion Biosensor for Cytokine Storm Biomarker Monitoring in Undiluted Biofluids Toward Wearable Applications. *Adv. Funct. Mater.* **2021**, *31*, 2005958.

(11) Wang, M.; Yang, Y.; Min, J.; Song, Y.; Tu, J.; Mukasa, D.; Ye, C.; Xu, C.; Heflin, N.; McCune, J. S.; Hsiai, T. K.; Li, Z.; Gao, W. A Wearable Electrochemical Biosensor for The Monitoring of Metabolites and Nutrients. *Nat. Biomed. Eng.* **2022**, *6*, 1−11.

(12) Hammock, M. L.; Knopfmacher, O.; Naab, B. D.; Tok, J. B.; Bao, Z. Investigation of Protein Detection Parameters Using Nanofunctionalized Organic Field-Effect Transistors. *ACS Nano* **2013**, *7* (5), 3970−3980.

(13) Liang, Y.; Xiao, M.; Wu, D.; Lin, Y.; Liu, L.; He, J.; Zhang, G.; Peng, L. M.; Zhang, Z. Wafer-Scale Uniform Carbon Nanotube Transistors for Ultrasensitive and Label-Free Detection of Disease Biomarkers. *ACS Nano* **2020**, *14* (7), 8866−8874.

(14) Hang, X.; He, S.; Dong, Z.; Li, Y.; Huang, Z.; Zhang, Y.; Sun, H.; Lin, L.; Li, H.; Wang, Y.; Liu, B.; Wu, N.; Ren, T.; Fan, Y.; Lou, J.; Yang, R.; Jiang, L.; Chang, L. High-Throughput DNA Tensioner Platform for Interrogating Mechanical Heterogeneity of Single Living Cells. *Small* **2022**, *18* (12), e2106196.

(15) Dong, Z.; Xue, X.; Liang, H.; Guan, J.; Chang, L. DNA Nanomachines for Identifying Cancer Biomarkers in Body Fluids and Cells. *Anal. Chem.* **2021**, *93* (4), 1855−1865.

(16) Siller, I. G.; Preuss, J. A.; Urmann, K.; Hoffmann, M. R.; Scheper, T.; Bahnemann, J. 3D-Printed Flow Cells for Aptamer-Based Impedimetric Detection of E. Coli Crooks Strain. *Sensors* **2020**, *20* (16), 4421.

(17) Zhang, X.; Song, C.; Yang, K.; Hong, W.; Lu, Y.; Yu, P.; Mao, L. Photoinduced Regeneration of An Aptamer-Based Electrochemical Sensor for Sensitively Detecting Adenosine Triphosphate. *Anal. Chem.* **2018**, *90* (8), 4968−4971.

(18) Zhou, Y.; Wu, Y.; Porholenko, O.; Grimsrud, M.; Sham, Y.; Papper, V.; Marks, R.; Steele, T. Aptamer Adaptive Binding Assessed By Stilbene Photoisomerization Towards Regenerating Aptasensors. *Sens. Actuators B Chem.* **2018**, *257*, 245−255.

(19) Forier, C.; Boschetti, E.; Ouhammouch, M.; Cibiel, A.; Ducongé, F.; Nogré, M.; Tellier, M.; Bataille, D.; Bihoreau, N.; Santambien, P.; Chtourou, Sami.; Perret, Gerald. DNA Aptamer Affinity Ligands for Highly Selective Purification of Human Plasma-

Related Proteins from Multiple Sources. *J. Chromatogr. A* **2017**, *1489*, 39−50.
(20) Hu, Y.; Cecconello, A.; Idili, A.; Ricci, F.; Willner, I. Triplex DNA Nanostructures: From Basic Properties to Applications. *Angew. Chem., Int. Ed. Engl.* **2017**, *56* (48), 15210−15233.
(21) Qi, X. J.; Lu, C. H.; Liu, X.; Shimron, S.; Yang, H. H.; Willner, I. Autonomous Control of Interfacial Electron Transfer and the Activation of DNA Machines by an Oscillatory pH System. *Nano Lett.* **2013**, *13* (10), 4920−4924.
(22) Lu, C. H.; Cecconello, A.; Elbaz, J.; Credi, A.; Willner, I. A Three-Station DNA Catenane Rotary Motor with Controlled Directionality. *Nano Lett.* **2013**, *13* (5), 2303−2308.
(23) Guo, W.; Lu, C. H.; Orbach, R.; Wang, F.; Qi, X. J.; Cecconello, A.; Seliktar, D.; Willner, I. pH-stimulated DNA Hydrogels Exhibiting Shape-Memory Properties. *Adv. Mater.* **2015**, *27* (1), 73−78.
(24) Porchetta, A.; Idili, A.; Vallée-Bélisle, A.; Ricci, F. General Strategy to Introduce pH-induced Allostery in DNA-based Receptors to Achieve Controlled Release of Ligands. *Nano Lett.* **2015**, *15* (7), 4467−4471.
(25) Yang, M.; Zhang, X.; Liu, H.; Kang, H.; Zhu, Z.; Yang, W.; Tan, W. Stable DNA Nanomachine Based on Duplex−Triplex Transition for Ratiometric Imaging Instantaneous pH Changes in Living Cells. *Anal. Chem.* **2015**, *87* (12), 5854−5859.
(26) Brunt, T. M.; Van Den Berg, J.; Pennings, E.; Venhuis, B. Adverse Effects of Levamisole in Cocaine Users: A Review and Risk Assessment. *Arch. Toxicol.* **2017**, *91* (6), 2303−2313.
(27) Pereira, R. B.; Andrade, P. B.; Valentão, P. A Comprehensive View of the Neurotoxicity Mechanisms of Cocaine and Ethanol. *Neurotox. Res.* **2015**, *28* (3), 253−267.
(28) Cekan, P.; Jonsson, E. O.; Sigurdsson, S. T. Folding of the Cocaine Aptamer Studied by EPR and Fluorescence Spectroscopies Using the Bifunctional Spectroscopic Probe Ç. *Nucleic Acids Res.* **2009**, *37* (12), 3990−3995.
(29) Porchetta, A.; Idili, A.; Vallée-Bélisle, A.; Ricci, F. General Strategy to Introduce pH-Induced Allostery in DNA-Based Receptors to Achieve Controlled Release of Ligands. *Nano Lett.* **2015**, *15* (7), 4467−4471.
(30) Stojanovic, M. N.; de Prada, P.; Landry, D. W. Aptamer-Based Folding Fluorescent Sensor for Cocaine. *J. Am. Chem. Soc.* **2001**, *123* (21), 4928−4931.
(31) Yang, C.; Wu, Q.; Liu, J.; Mo, J.; Li, X.; Liu, Z.; Yang, J.; Jiang, L.; Chen, W.; Chen, H. J.; Wang, J.; Xie, X. Intelligent Wireless Theranostic Contact Lens for Electrical Sensing and Regulation of Intraocular Pressure. *Nat. Commun.* **2022**, *13* (1), 2556.
(32) Wang, T.; Wang, M.; Wang, J.; Yang, L.; Ren, X.; Song, G.; Chen, S.; Yuan, Y.; Liu, R.; Pan, L.; Li, Z.; Leow, W. R.; Luo, Y.; Ji, S.; Cui, Z.; He, K.; Zhang, F.; Lv, F.; Tian, Y.; Cai, K.; Yang, B.; Niu, J.; Zou, H.; Liu, S.; Xu, G.; Fan, X.; Hu, B.; Loh, X. J.; Wang, L.; Chen, X. A Chemically Mediated Artificial Neuron. *Nat. Electron.* **2022**, *5*, 1−10.
(33) Strehlitz, B.; Reinemann, C.; Linkorn, S.; Stoltenburg, R. Aptamers for Pharmaceuticals and Their Application in Environmental Analytics. *Bioanal. Rev.* **2012**, *4* (1), 1−30.
(34) Chu, C. H.; Sarangadharan, I.; Regmi, A.; Chen, Y. W.; Hsu, C. P.; Chang, W. H.; Lee, G. Y.; Chyi, J. I.; Chen, C. C.; Shiesh, S. C.; Lee, G. B.; Wang, Y. L. Beyond the Debye Length in High Ionic Strength Solution: Direct Protein Detection with Field-Effect Transistors (FETs) in Human Serum. *Sci. Rep.* **2017**, *7* (1), 5256.
(35) Lee, D.; Jung, W. H.; Lee, S.; Yu, E. S.; Lee, T.; Kim, J. H.; Song, H. S.; Lee, K. H.; Han, S. K.; Choi, M. C.; Ahn, D. J.; Ryu, Y. S.; Kim, C. Ionic Contrast Across a Lipid Membrane for Debye Length Extension: Towards an Ultimate Bioelectronic Transducer. *Nat. Commun.* **2021**, *12* (1), 3741.
(36) Purwidyantri, A.; Domingues, T.; Borme, J.; Guerreiro, J. R.; Ipatov, A.; Abreu, C. M.; Martins, M.; Alpuim, P.; Prado, M.Influence of the Electrolyte Salt Concentration on DNA Detection with Graphene Transistors. *Biosensors (Basel)***2021**, *11* (1), 24.
(37) Sun, J.; Liu, Y.Matrix Effect Study and Immunoassay Detection Using Electrolyte-Gated Graphene Biosensor. *Micromachines (Basel)* **2018**, *9* (4), 142.
(38) Chen, H.; Xiao, M.; He, J.; Zhang, Y.; Liang, Y.; Liu, H.; Zhang, Z. Aptamer-Functionalized Carbon Nanotube Field-Effect Transistor Biosensors for Alzheimer's Disease Serum Biomarker Detection. *ACS sensors* **2022**, *7*, 2075−2083.
(39) Nakatsuka, N.; Abendroth, J. M.; Yang, K. A.; Andrews, A. M. Divalent Cation Dependence Enhances Dopamine Aptamer Biosensing. *ACS Appl. Mater. Interfaces* **2021**, *13* (8), 9425−9435.
(40) Nello, F.; Jolly, P.; Bhalla, N.; Cromhout, M.; Flanagan, S. P.; Fogel, R.; Limson, J. L.; Estrela, P. Optimisation of an Electrochemical Impedance Spectroscopy Aptasensor by Exploiting Quartz Crystal Microbalance with Dissipation Signals. *Sens. Actuators B Chem.* **2015**, *220*, 369−375.
(41) Aliakbarinodehi, N.; Jolly, P.; Bhalla, N.; Miodek, A.; De Micheli, G.; Estrela, P.; Carrara, S. Aptamer-based Field-Effect Biosensor for Tenofovir Detection. *Sci. Rep.* **2017**, *7*, 44409.
(42) Wang, J.; Hou, J.; Zhang, H.; Tian, Y.; Jiang, L. Single Nanochannel-Aptamer-Based Biosensor for Ultrasensitive and Selective Cocaine Detection. *ACS Appl. Mater. Interfaces* **2018**, *10* (2), 2033−2039.
(43) Matsui, A.; Alvarez, V. A. Cocaine Inhibition of Synaptic Transmission in The Ventral Pallidum Is Pathway-Specific and Mediated by Serotonin. *Cell Rep.* **2018**, *23* (13), 3852−3863.
(44) Bhattacharyya, D.; Mirihana Arachchilage, G.; Basu, S. Metal Cations in G-Quadruplex Folding and Stability. *Front. Chem.* **2016**, *4*, 38.
(45) Borges, C. R.; Roberts, J. C.; Wilkins, D. G.; Rollins, D. E. Cocaine, Benzoylecgonine Amphetamine, and N-Acetylamphetamine Bincling to Melanin Subtypes. *J. Anal. Toxicol.* **2003**, *27* (3), 125−134.
(46) National Institutes of Health National Library of Medicine. https://pubchem.ncbi.nlm.nih.go -v/compound/Cocaine (accessed 2022−03−24).
(47) D'Aurelio, R.; Chianella, I.; Goode, J. A.; Tothill, I. E.Molecularly Imprinted Nanoparticles Based Sensor for Cocaine Detection. *Biosensors (Basel)***2020**, *10* (3), 22.
(48) Pusomjit, P.; Teengam, P.; Thepsuparungsikul, N.; Sanongkiet, S.; Chailapakul, O. Impedimetric Determination of Cortisol Using Screen-Printed Electrode with Aptamer-Modified Magnetic Beads. *Mikrochim. Acta* **2021**, *188* (2), 41.
(49) Tsai, M. Y.; Creedon, N.; Brightbill, E.; Pavlidis, S.; Brown, B.; Gray, D. W.; Shields, N.; Sayers, R.; Mooney, M. H.; O' Riordan, A.; Vogel, E. M. Direct Correlation Between Potentiometric and Impedance Biosensing of Antibody-Antigen Interactions Using an Integrated System. *Appl. Phys. Lett.* **2017**, *111* (7), 073701.
(50) McConnell, E. M.; Bolzon, R.; Mezin, P.; Frahm, G.; Johnston, M.; DeRosa, M. C. PHAST (Ph-Driven Aptamer Switch for Thrombin) Catch-and-Release of Target Protein. *Bioconjugate Chem.* **2016**, *27* (6), 1493−1499.
(51) Gordon, C. K.; Eisenstein, M.; Soh, H. T. Direct Selection Strategy for Isolating Aptamers with Ph-Sensitive Binding Activity. *ACS Sens.* **2018**, *3* (12), 2574−2580.
(52) Hemmatian, Z.; Jalilian, E.; Lee, S.; Strakosas, X.; Khademhosseini, A.; Almutairi, A.; Shin, S. R.; Rolandi, M. Delivery of Cargo with a Bioelectronic Trigger. *ACS Appl. Mater. Interfaces* **2018**, *10* (26), 21782−21787.
(53) Strakosas, X.; Selberg, J.; Zhang, X.; Christie, N.; Hsu, P. H.; Almutairi, A.; Rolandi, M. A Bioelectronic Platform Modulates pH in Biologically Relevant Conditions. *Adv. Sci. (Weinh)* **2019**, *6* (7), 1800935.
(54) Strakosas, X.; Selberg, J.; Pansodtee, P.; Yonas, N.; Manapongpun, P.; Teodorescu, M.; Rolandi, M. A Non-Enzymatic Glucose Sensor Enabled by Bioelectronic pH Control. *Sci. Rep.* **2019**, *9* (1), 10844.
(55) Liu, Y.; Pharr, M.; Salvatore, G. A. Lab-on-skin: A Review of Flexible and Stretchable Electronics for Wearable Health Monitoring. *ACS Nano* **2017**, *11* (10), 9614−9635.

https://doi.org/10.1021/acsnano.2c08511
ACS Nano 2022, 16, 20922−20936

(56) Kurs, A.; Karalis, A.; Moffatt, R.; Joannopoulos, J. D.; Fisher, P.; Soljacic, M. Wireless Power Transfer via Strongly Coupled Magnetic Resonances. *Science* **2007**, *317* (5834), 83−86.
(57) Koo, J.; Kim, S. B.; Choi, Y. S.; Xie, Z.; Bandodkar, A. J.; Khalifeh, J.; Yan, Y.; Kim, H.; Pezhouh, M. K.; Doty, K.; Lee, G.; Chen, Y.; Lee, S.; Andrea, D.; Jung, K.; Lee, K.; Li, K.; Jo, S.; Wang, H.; Kim, J. H.; Kim, J.; Choi, S.; Jang, W.; Oh, Y.; Park, I.; Kwak, S.; Park, J.; Hong, D.; Feng, X.; Lee, C. H.; Banks, A.; Leal, C.; Lee, H. M.; Huang, Y.; Franz, C. K.; Ray, W.; MacEwan, M.; Kang, S. K.; Roger, J. A. Wirelessly Controlled, Bioresorbable Drug Delivery Device with Active Valves That Exploit Electrochemically Triggered Crevice Corrosion. *Sci. Adv.* **2020**, *6* (35), eabb1093.
(58) Huang, Y.; Li, H.; Hu, T.; Li, J.; Yiu, C. K.; Zhou, J.; Huang, X.; Yao, K.; Qiu, X.; Zhou, Y.; Li, D.; Zhang, B.; Shi, R.; Liu, Y.; Wong, T. H.; Wu, M.; Jia, H.; Gao, Z.; Zhang, Z.; He, J.; Zheng, M.; Song, E.; Wang, L.; Xu, C.; Yu, X. Implantable Electronic Medicine Enabled by Bioresorbable Microneedles for Wireless Electrotherapy and Drug Delivery. *Nano Lett.* **2022**, *22* (14), 5944−5953.
(59) Koo, J.; MacEwan, M. R.; Kang, S. K.; Won, S. M.; Stephen, M.; Gamble, P.; Xie, Z.; Yan, Y.; Chen, Y. Y.; Shin, J.; Birenbaum, N.; Chung, S.; Kim, S. B.; Khalifeh, J.; Harburg, D. V.; Bean, K.; Paskett, M.; Kim, J.; Zohny, Z. S.; Lee, S. M.; Zhang, R.; Luo, K.; Ji, B.; Banks, A.; Lee, H. M.; Huang, Y.; Ray, W. Z.; Rogers, J. A. Wireless bioresorbable electronic system enables sustained nonpharmacological neuroregenerative therapy. *Nat. Med.* **2018**, *24* (12), 1830−1836.
(60) Guo, Q.; Koo, J.; Xie, Z.; Avila, R.; Yu, X.; Ning, X.; Zhang, H.; Liang, X.; Kim, S. B.; Yan, Y.; MacEwan, M. R.; Lee, H. M.; Song, A.; Di, Z.; Huang, Y.; Mei, Y.; Roger, J. A. A Bioresorbable Magnetically Coupled System for Low-Frequency Wireless Power Transfer. *Adv. Funct. Mater.* **2019**, *29* (46), 1905451.
(61) Yang, S.; Chen, Y. C.; Nicolini, L.; Pasupathy, P.; Sacks, J.; Su, B.; Yang, R.; Sanchez, D.; Chang, Y. F.; Wang, P.; Schnyer, D.; Neikirk, D.; Lu, N. "Cut-and-Paste" Manufacture of Multiparametric Epidermal Sensor Systems. *Adv. Mater.* **2015**, *27* (41), 6423−6430.

Recommended by ACS

Artificial Nucleotide Aptamer-Based Field-Effect Transistor for Ultrasensitive Detection of Hepatoma Exosomes
Yiheng Chen, Dacheng Wei, *et al.*
DECEMBER 28, 2022
ANALYTICAL CHEMISTRY
READ

Total Bioaerosol Detection by Split Aptamer-Based Electrochemical Nanosensor Chips
Rui Zhang, Meng Liu, *et al.*
NOVEMBER 15, 2022
ANALYTICAL CHEMISTRY
READ

Thermodynamic and Kinetic Modulation of Microfluidic Interfaces by DNA Nanoassembly Mediated Merit-Complementary Heteromultivalency
Jiajun Ling, Yanling Song, *et al.*
NOVEMBER 23, 2022
ACS NANO
READ

Universal and Flexible Signal Transduction Module Based on Overload Triggering Probe Escape for Sensitive Detection of Tau Protein
Chengjie Duan, Yang Xiang, *et al.*
SEPTEMBER 07, 2022
ANALYTICAL CHEMISTRY
READ

Get More Suggestions >

https://doi.org/10.1021/acsnano.2c08511
ACS Nano 2022, 16, 20922−20936